Cell Reports, Volume *20*

Supplemental Information

Circadian and Feeding Rhythms Orchestrate the Diurnal Liver Acetylome

Daniel Mauvoisin, Florian Atger, Loïc Dayon, Antonio Núñez Galindo, Jingkui Wang, Eva Martin, Laetitia Da Silva, Ivan Montoliu, Sebastiano Collino, Francois-Pierre Martin, Joanna Ratajczak, Carles Cantó, Martin Kussmann, Felix Naef, and Frédéric Gachon

Supplemental Information

Supplemental Figures

Figure S1. Experimental design and data quality check, related to Figure 1

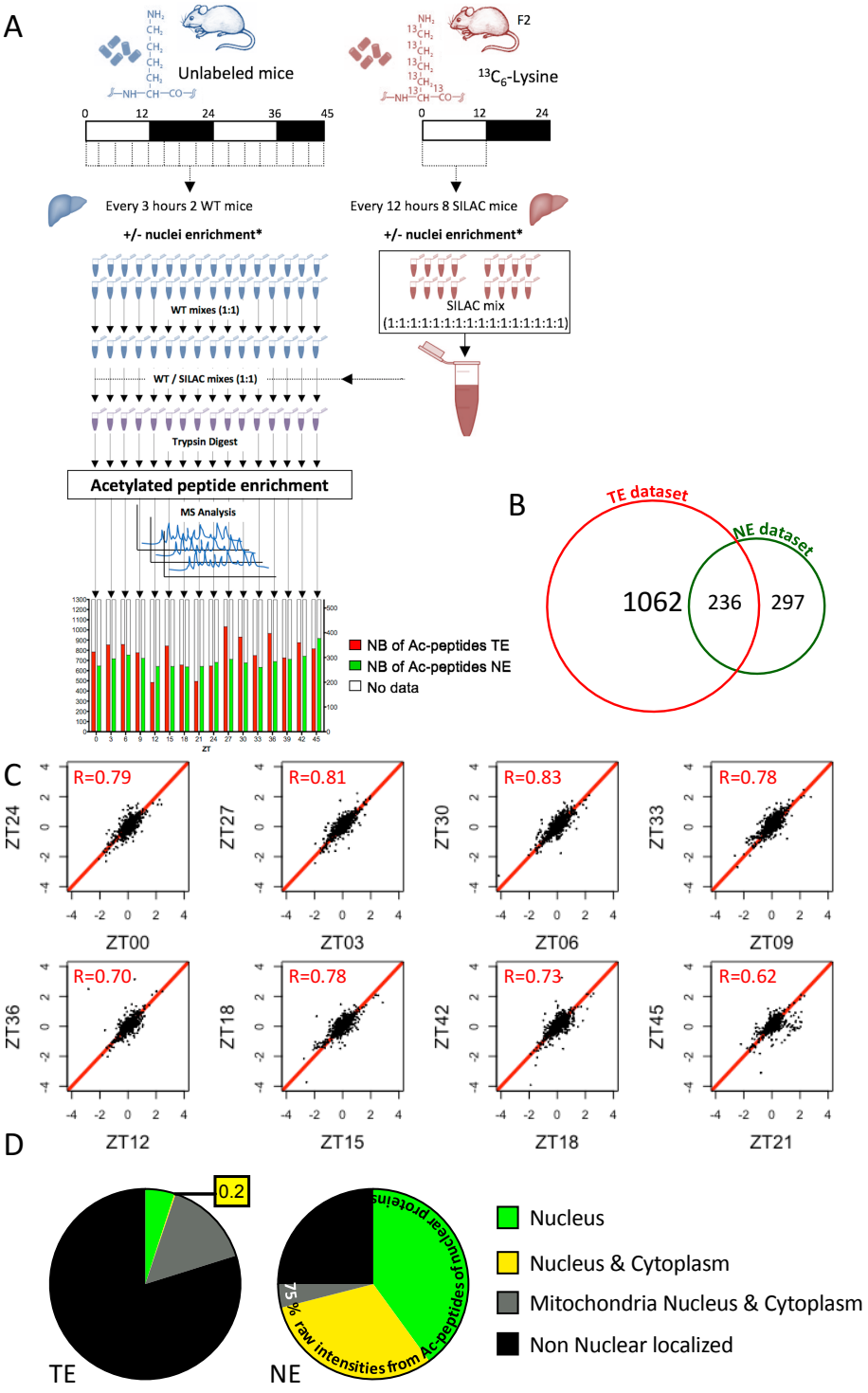

A. Workflow of the SILAC-based MS analysis of acetylated proteins from total mouse liver extracts (TE) and purified nuclei (NE). The lower graph represents the number of acetylation sites for each time point in TE (black bars, left Y axis) and NE (red bars, right Y axis).
B. Number of acetylated sites quantified in TE (red circle, 1298 acetylated sites identified) and NE (green circle, 533 acetylated sites identified).
C. Pearson correlation analysis of biological replicates at the eight time points. All values are log2 ratios to the common reference samples. The biological replicates are well correlated (76% average Pearson correlation) and showed similar spread, indicating that the quality of the protein purifications was fairly homogenous.
D. Fractions of raw intensity signals quantified with SILAC-MS for nuclear and non-nuclear located proteins in TE (left graph) and NE (right graph).

Figure S2. Overlap of rhythmic acetylation sites and expression of Acetyl-CoA synthesizing enzymes, related to Figure 2

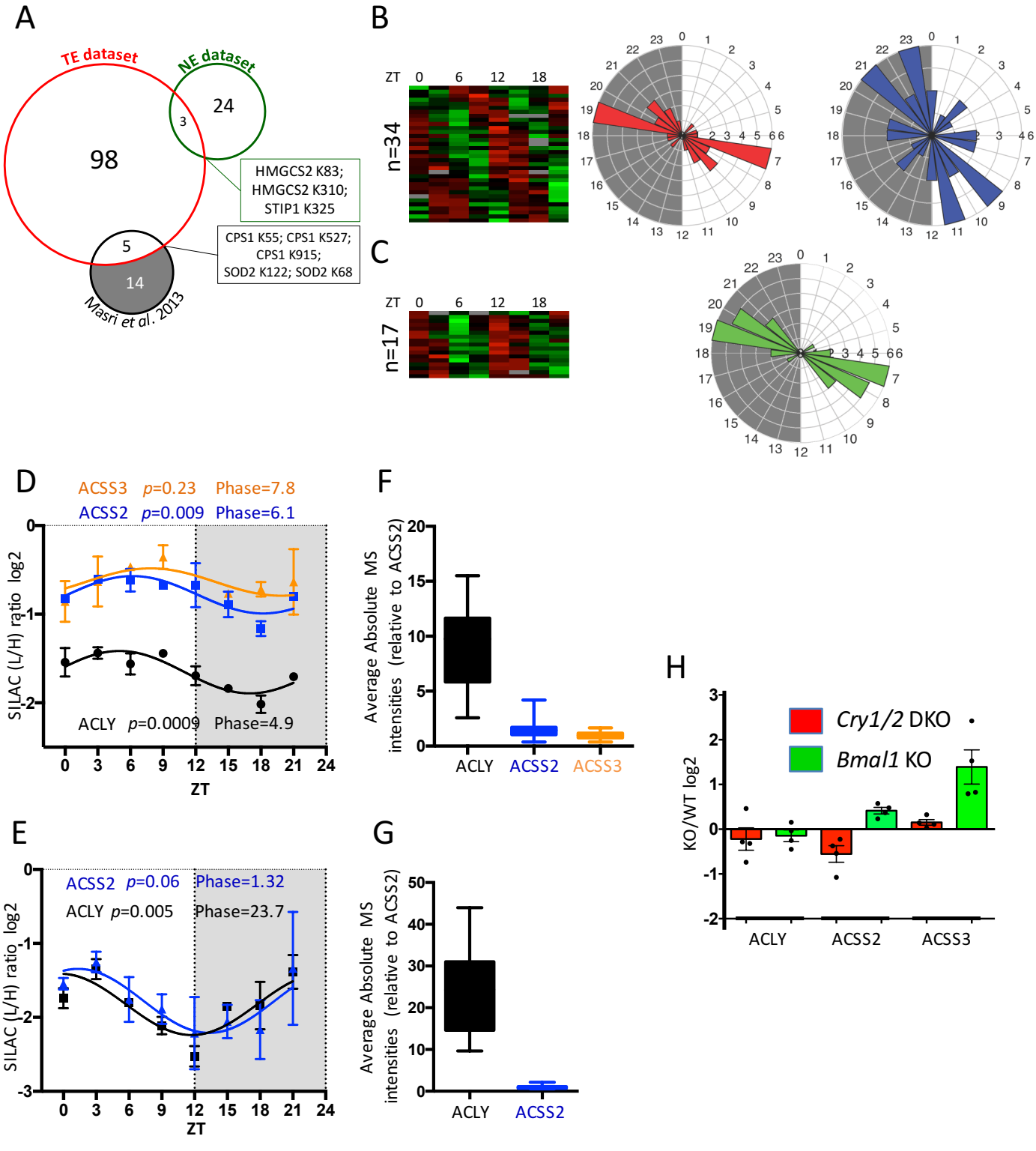

A. Venn diagram showing the overlap of rhythmic acetylation sites between the TE dataset (106 rhythmic acetylation sites), the NE dataset (27 rhythmic acetylation sites), and the dataset of (Masri et al., 2013) (19 rhythmic acetylation sites).
B-C. Heat maps showing 12 hours rhythmic acetylation sites normalized by their corresponding total protein amount in (B) TE (n=34) and (C) NE (n=17) under light-dark and night-restricted feeding conditions. Data were standardized by rows and gray blocks indicate missing protein data. The polar plots on the right of each heatmap display peak phase distribution of the 12 hours rhythmic acetylation sites in each extract. Colors indicate acetylation sites with a corresponding total protein having a defined mitochondrial (n=17 sites; red) or cytoplasmic (n=20 sites; blue) localization in TE, or acetylation sites from NE (n=17; green).
D-E. Temporal protein expression of ACLY (black), ACSS2 (blue), and ACSS3 (orange) in TE (D) and NE (E) (ACSS3 not detected in NE). The values represent the mean ± SEM from two independent biological samples.
F-G. Raw intensity signals quantified by SILAC-MS for ACLY (black), ACSS2 (blue), and ACSS3 (orange) in TE (F) and NE (G) (ACSS3 not detected in NE). Data are expressed relative to ACSS2 average signal, error bars represent min to max.
H. Differential protein expression level of ACLY, ACSS2, and ACSS3 in TE in *Cry1/2* DKO mice (red bars) and *Bmal1* KO mice (green bars) compared to respective WT animals. Data show average level ± SEM in four samples collected around the clock.
Data of panels D, F, H, and E, G are from (Mauvoisin et al., 2014) and (Wang et al., 2017), respectively.

Figure S3. Temporal nuclear expression of SIRT1 and SIRT7, related to Figure 3

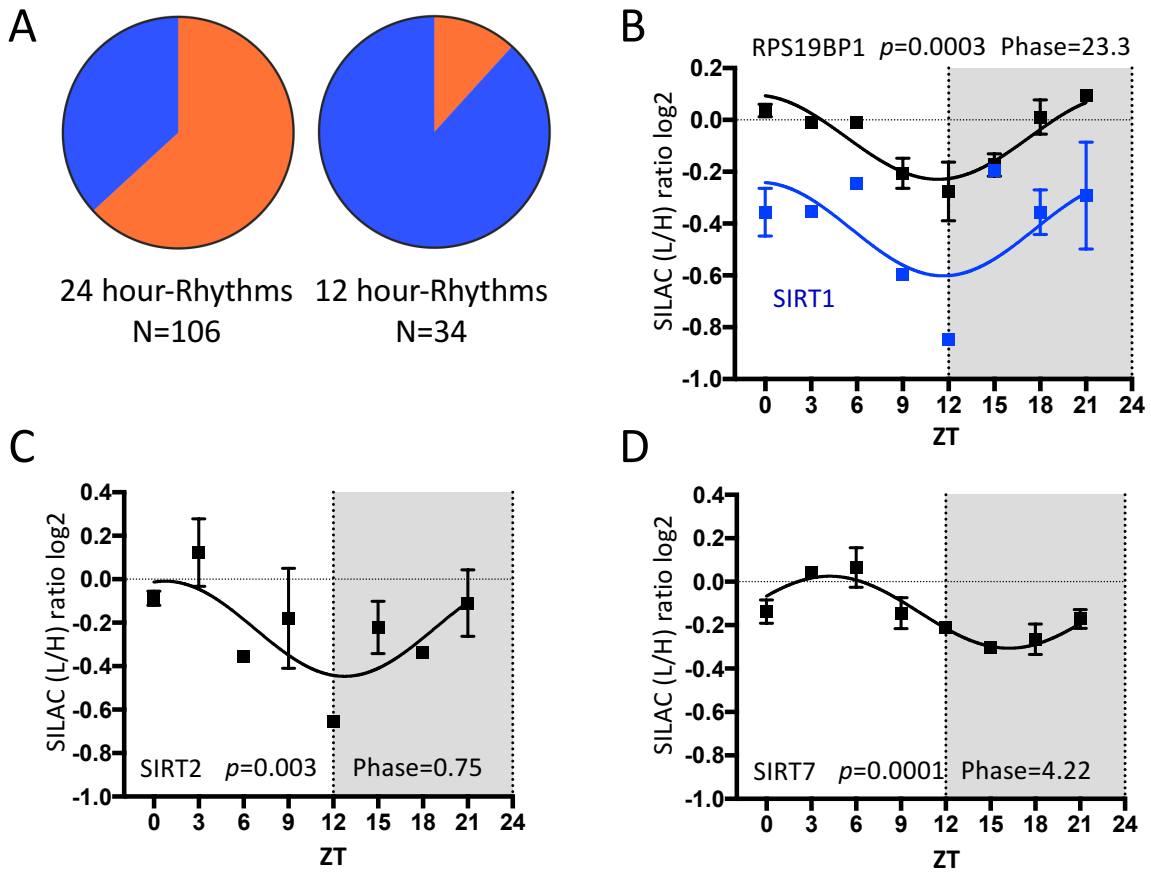

A. Proportion of SIRT3 targets (orange) versus non-SIRT3 targets (blue) in rhythmic acetylation sites with 24 hour-rhythms and 12 hour-rhythms.
B. Temporal nuclear expression of SIRT1 (blue) and its coactivator RPS19BP1 (black).
C. Temporal nuclear expression of SIRT2.
D. Temporal nuclear expression of SIRT7.
For B, C, and D, the values represent the mean ± SEM from two independent biological samples. Data are extracted from (Wang et al., 2017).

Figure S4. Additional metabolic pathways affected by rhythmic acetylation, related to Figure 5

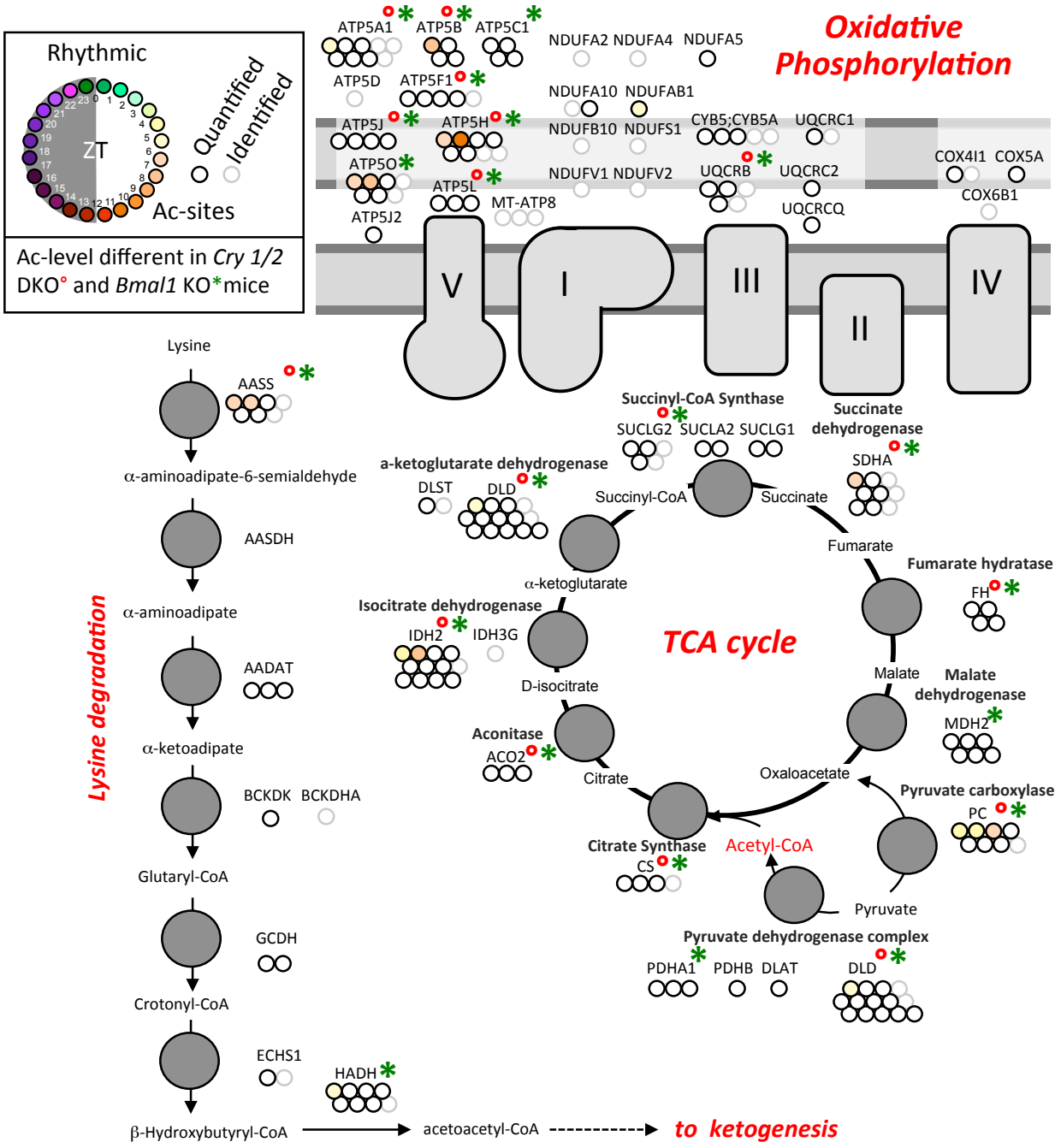

Rhythmic protein acetylation and their regulation by the circadian clock for lysine degradation, oxidative phosphorylation, and TCA cycle pathways. Each dot represents a unique acetylation site within the protein of interest. Grey and black dots represent non-rhythmic identified and quantified acetylation sites, respectively, whereas phase of rhythmic acetylation sites are color-coded. Superscripted red dots and green asterisks indicate protein acetylation level significantly different in *Cry1/2* DKO and *Bmal1* KO mice, respectively.

Figure S5. Differential acetylation of the enzymes involved in the different metabolic pathways in *Cry1/2* and *Bmal1* KO mice, related to Figure 5 and S4

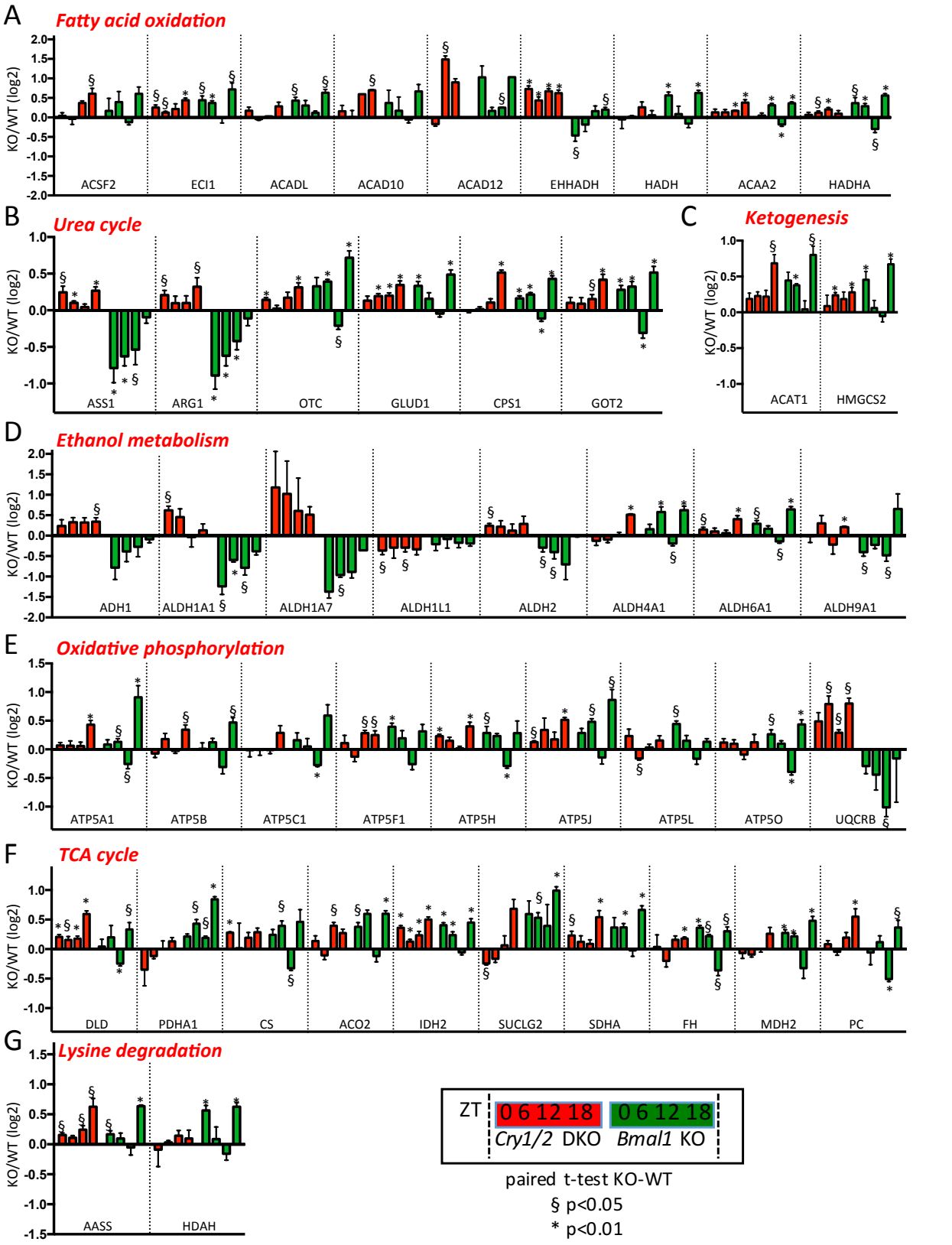

Differential temporal acetylation level of proteins implicated in the metabolic pathways presented in Figures 5 and S4: (A) Fatty acid oxidation; (B) Urea cycle; (C) Ketogenesis; (D) Ethanol metabolism; (E) Oxidative phosphorylation; (F) TCA cycle; and (G) Lysine degradation. Data shown for each protein represents mean differential level of global protein acetylation between *Cry1/2* DKO (red bars), *Bmal1* KO (green bars) and their corresponding WT controls (mean ± SEM of acetylation sites log2 difference). Paired student t-test was performed to compare global acetylation level of each protein between KO mice and their respective WT controls.

Figure S6. Impact of rhythmic acetylation on metabolites levels on additional pathways, related to Figure 6

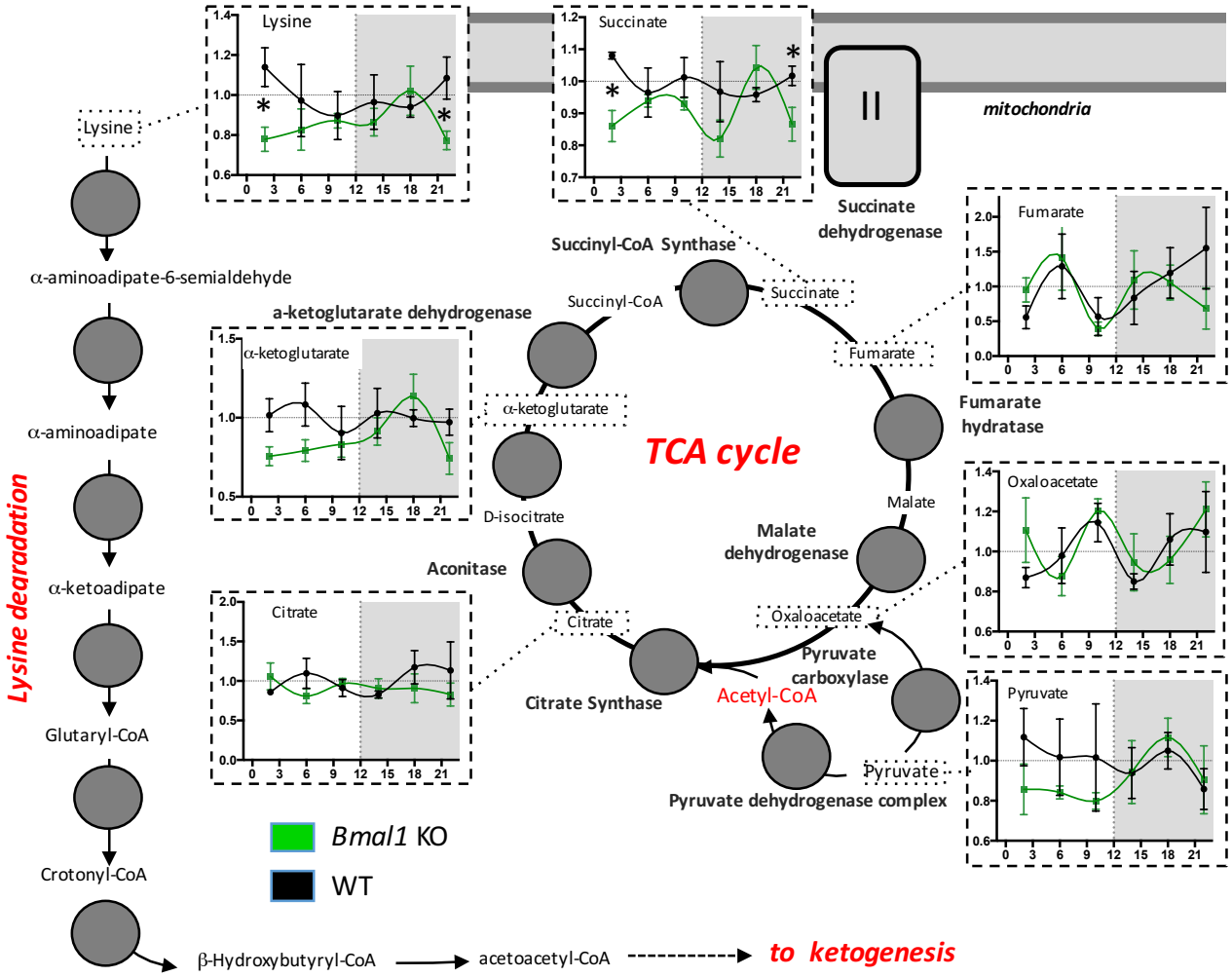

Liver temporal profiles of metabolites in *Bmal1* KO (green line) and WT littermates (black line). Data are expressed relative to the temporal mean of WT values ± SEM. The analysis concerned key metabolites of Lysine degradation and TCA cycle. Student t-test was performed to compare the average level of metabolites at every time point between the different genotypes (n=4). * indicate $p<0.05$ between *Bmal1* KO and WT mice.

Supplemental Experimental Procedures

Total protein extraction

Livers were homogenized in a lysis buffer containing 8M Urea, a protease inhibitor cocktail (cOmplete ULTRA®, Roche), a phosphatase inhibitor cocktail (PhosphoSTOP®, Roche), and HDAC and SIRTUIN inhibitors (AGK7, salermide, and trichostatin A, all from SantaCruz Biochemicals). After 20 min incubation on ice, extracts were centrifuged 10 min at 20,000 g. The supernatants were harvested and the resulting total protein extracts (TE) were quantified using a BCA protein assay kit (Thermo Scientific).

Nuclear protein extraction

Livers were homogenized in sucrose homogenization buffer containing 2.2 M sucrose, 15 mM KCl, 2 mM EDTA, 10 mM HEPES (pH 7.6), 0.15 mM spermin, 0.5 mM spermidin, 1 mM DTT, and protease inhibitors (0.5 mM PMSF, 10 mg/ml Aprotinin, 0.7 mg/ml Pepstatin A, and 0.7 mg/ml Leupeptin). Lysates were deposited on a sucrose cushion containing 2.05 M sucrose, 10 % glycerol, 15 mM KCl, 2 mM EDTA, 10 mM HEPES (pH 7.6), 0.15 mM spermin, 0.5 mM spermidin, 1 mM DTT, and protease inhibitors. After 45 min of centrifugation at 105,000 g at 4 °C, the nuclei pellets were suspended in a buffer composed of 10 mM HEPES (pH 7.6), 100 mM KCl, 0.1 mM EDTA, 10 % Glycerol, 0.15 mM spermine, 0.5 mM spermidine, 0.1 mM NaF, 0.1 mM sodium orthovanadate, 0.1 mM ZnSO4, 1 mM DTT, and protease inhibitors. This constitutes the purified nuclei fractions. Nuclear protein extracts were obtained by adding an equal volume of NUN buffer (2 M urea, 600 mM NaCl, 50 mM HEPES (pH 7.6), 1 mM DTT, a protease inhibitor cocktail (cOmplete ULTRA®), a phosphatase inhibitor cocktail (PhosphoSTOP®), and HDAC and SIRTUIN inhibitors (AGK7, salermide, and trichostatin A) followed by a 20 min incubation on ice. The supernatants resulting from a 10 min centrifugation at 21,000g at 4 °C constitute the nuclear extracts (NE). Protein extracts were quantified using a BCA protein assay kit (Thermo Scientific).

Analysis of acetylation by RP-LC MS/MS

Sample preparation for proteomic analysis

Equal amounts of proteins from TE or NE from 2 non-SILAC mice were pooled for each of the 16 time points (every 3 hours for 45 hours; WT mix). A complex and common reference SILAC protein mix (SILAC mix) was prepared from 16 SILAC protein samples (6 SILAC male and 10 SILAC female livers) collected at ZT0 and ZT12 (Fig S1A). Thereafter, the 16 mixes were obtained by adding the same amount of SILAC mix (250 µg for TE, and 175 µg for NE) to the WT mixes (125+125=250 µg for TE, and 87.5+87.5=175 µg for NE). An equivalent procedure was applied for the 4 *Cry1/2* DKO, the 4 *Bmal1* KO mice, and their 4 WT littermates protein samples collected every 6 hours for 24 hours (the same SILAC mix was used as a reference). Mixed heavy/light extracts representing each experimental condition (Fig S1A) were processed in parallel. Protein disulfide bridges were reduced with 10 mM tris (2-carboxyethyl) phosphine hydrochloride for 1 hour at 55 °C. Alkylation was performed with 17 mM Iodoacetamide for 30 min at room temperature in the dark. To remove lipids and salts, proteins were precipitated using methanol/chloroform. Briefly, methanol, then chloroform and water for adjusting final volume were added. Mixtures were centrifuged at 13,000 rpm for 5 min at 4 °C. Upper phases were discarded. The white precipitates were additionally washed with methanol prior to be dried for 5 min. Remaining pellets were suspended in 100 mM triethylammonium hydrogen carbonate buffer pH 8.5 and proteins were digested, first with Lys-C (1:100 *w*/*w*) (Promega) at 37 °C for 5 hours and then overnight with Trypsin (1:100 *w*/*w*) (Promega). Samples were cleaned up using Oasis HLB cartridges (Waters) and finally dried. Purified peptides were dissolved in the immunoprecipitation buffer (PTM Biolabs) for acetylated-lysine enrichment. A volume of 15 µL of drained anti-acetyl lysine antibody beaded agarose (PTM Biolabs) was washed with cold phosphate buffer saline. Peptides and washed beads were mixed and incubated overnight with gentle end-to-end rotation at 4 °C. The beads were centrifuged and the supernatant was discarded. After sequential washing of the beads with wash buffer I (PTM Biolabs) (3 times), wash buffer II (PTM Biolabs), and water (twice), the anti-acetyl lysine enriched peptides were eluted from the beads with elution buffer (PTM Biolabs), further dried and spin filtered (0.22 µm).

RP-LC MS/MS

The samples were dissolved in 25 µL H_2O/CH_3CN/Formic Acid 96.9/3/0.1 for RP-LC MS/MS analysis. RP-LC MS/MS was performed on a hybrid linear ion trap-Orbitrap (LTQ-OT) Elite equipped with an Ultimate 3000 RSLC nano system (Thermo Fisher Scientific). Proteolytic peptides (injection of 5 µL of sample) were trapped on an Acclaim PepMap 75 µm × 2 cm (C18, 3 µm, 100 Å) pre-column and separated on an Acclaim PepMap RSLC 75 µm × 50 cm (C18, 2 µm, 100 Å) column (Thermo Fisher Scientific) coupled to a stainless steel nanobore emitter (40 mm, OD 1/32") mounted on a Nanospray Flex Ion Source (Thermo Fisher Scientific). The analytical separation was run for 150 min using a gradient that reached 30% of CH_3CN after 140 min and 80% of CH_3CN after 150 min at a flow rate of 220 nl/min. For MS survey scans, the OT resolution was 120,000 (ion population of 1.10^6) with an *m/z* window from

300 to 1,500. For MS/MS with collision-induced dissociation at 30 % of the normalized collision energy, ion population was set to 1.10^4 (isolation width of 2 *m/z*), and a maximum injection time of 150 ms in the LTQ. A maximum of 20 precursor ions (most intense) were selected for MS/MS. Dynamic exclusion was set for 60 within a ± 5 ppm window. A lock mass of *m/z* = 445.1200 was used. Each sample was analyzed in triplicate.

Data processing and analysis

MaxQuant (version 1.4.1.2) (Cox and Mann, 2008) was used for data processing. Identification was performed using Andromeda (Cox et al., 2011) as search engine against the mouse UniProtKB database (26/06/2013 release; 50818 entries). Variable amino acid modifications were acetyl (K), acetyl (N-term), and oxidation (M). Carbamidometyl (C) was set as fixed modification. Trypsin/P (*i.e.*, cleaves after lysine and arginine also if a proline follows) was selected as the proteolytic enzyme, with a maximum of two potential missed cleavages (four missed cleavages parameter was also assessed but without any improvement on the results). Peptide and fragment ion tolerance were set to, respectively, 6 ppm and 0.5 Da. Peptide-spectrum match, protein and site false discovery rates (FDRs) were fixed at 1% against a reversed sequence database. Quantification was performed with stable isotope with a multiplicity of 2 using Lysine $^{13}C_6$ as heavy labels. A maximum of 3 labeled amino acids per peptide was specified. Site quantification used least modified peptide.

The mass spectrometry proteomic data have been deposited to the ProteomeXchange Consortium *via* the PRIDE (Vizcaíno et al., 2016) partner repository with the dataset identifiers PXD005317 and PXD005310 for TE and NE respectively.

^{1}H NMR spectroscopic analysis of liver Metabonome

Frozen liver samples (~40-60 mg) were homogenized in 650 µl of ice-cold methanol. Homogenates were incubated on ice for 15 min and then supplemented with ice-cold chloroform (650 µl), vortexed thoroughly, and incubated on ice for 15 min. Hence, 650 µl of water was added to each samples, vortexed thoroughly, and incubated overnight at -20 °C. Phase separation was performed by centrifugation at 13,000 g and 4 °C for 40 min. The upper soluble phases were collected and evaporated. The dried mouse liver extracts were homogenized in 700 µl of phosphate buffer solution (0.2 M $NaHPO_4$ pH 7.0, 90 % D_2O, 10 % H_2O) containing TSP (0.5 mM, reference signal at $\delta = 0$). After centrifugation, a volume of 600 µl was transferred into 5 mm diameter NMR tubes by using a Gilson robot (Gilson AG). ^{1}H NMR spectra were then recorded on a 600 MHz Avance II Bruker NMR spectrometer equipped with a 5 mm PATXI probe (Bruker Biospin) operating at 600.13 MHz and 300 K. Standard ^{1}H NMR one-dimensional pulse sequence with water suppression and Carr-Purcell-Meiboom-Gill (CPMG) spin-echo sequence with water suppression were acquired using 128 scans with 98 K data-points. Processing of ^{1}H NMR spectra was carried out using TOPSPIN 3.2 software package (Bruker Biospin). The spectral data (from $\delta = 0.4$ to $\delta = 10$) were imported into Matlab (version R2013b) and normalized to total area after solvent peak removal. Poor quality or highly diluted spectra were discarded from the subsequent analysis. Based on metabolic pathways of interest, representative signals of metabolites assignable on ^{1}H NMR spectra were integrated. The signals were expressed in arbitrary unit corresponding to a peak area normalized to total tissue metabolic profile, which is representative of relative change in metabolite concentration in the tissue.

References for antibodies used for Western Blotting

NRK1 antibodies were previously described (Ratajczak et al., 2016). Rabbit anti-SOD2/MnSOD (ab68155) and anti-SOD2/MnSOD (acetyl K68) (ab137037) antibodies were from Abcam. Rabbit anti-acetyl-lysine antibody (PTM-105), rabbit anti-succinyl-lysine antibody (PTM-401) and rabbit anti-malonyl-lysine antibody (PTM-901) were from PTM Biolabs.

Supplemental References

Cox, J., and Mann, M. (2008). MaxQuant enables high peptide identification rates, individualized p.p.b.-range mass accuracies and proteome-wide protein quantification. Nat Biotechnol 26, 1367-1372.

Cox, J.r., Neuhauser, N., Michalski, A., Scheltema, R.A., Olsen, J.V., and Mann, M. (2011). Andromeda: A Peptide Search Engine Integrated into the MaxQuant Environment. J Proteome Res 10, 1794-1805.

Masri, S., Patel, V.R., Eckel-Mahan, K.L., Peleg, S., Forne, I., Ladurner, A.G., Baldi, P., Imhof, A., and Sassone-Corsi, P. (2013). Circadian acetylome reveals regulation of mitochondrial metabolic pathways. Proc Natl Acad Sci U S A 110, 3339-3344.

Mauvoisin, D., Wang, J., Jouffe, C., Martin, E., Atger, F., Waridel, P., Quadroni, M., Gachon, F., and Naef, F. (2014). Circadian clock-dependent and -independent rhythmic proteomes implement distinct diurnal functions in mouse liver. Proc Natl Acad Sci U S A 111, 167-172.

Ratajczak, J., Joffraud, M., Trammell, S.A.J., Ras, R., Canela, N., Boutant, M., Kulkarni, S.S., Rodrigues, M., Redpath, P., Migaud, M.E., Auwerx, J., Yanes, O., Brenner, C., and Cantó, C. (2016). NRK1 controls nicotinamide mononucleotide and nicotinamide riboside metabolism in mammalian cells. Nature Commun 7, 13103.

Vizcaíno, J.A., Csordas, A., del-Toro, N., Dianes, J.A., Griss, J., Lavidas, I., Mayer, G., Perez-Riverol, Y., Reisinger, F., Ternent, T., Xu, Q.-W., Wang, R., and Hermjakob, H. (2016). 2016 update of the PRIDE database and its related tools. Nucleic Acids Res 44, D447-D456.

Wang, J., Mauvoisin, D., Martin, E., Atger, F., Galindo, A.N., Dayon, L., Sizzano, F., Palini, A., Kussmann, M., Waridel, P., Quadroni, M., Dulić, V., Naef, F., and Gachon, F. (2017). Nuclear Proteomics Uncovers Diurnal Regulatory Landscapes in Mouse Liver. Cell Metab 25, 102-117.